ORIGINAL   **Open Access**

X-ray imaging technique using colloid solution of Au/silica core-shell nanoparticles

Yoshio Kobayashi[1*], Hiromitsu Inose[1], Tomohiko Nakagawa[2], Yohsuke Kubota[2], Kohsuke Gonda[2] and Noriaki Ohuchi[2]

Abstract

This work describes X-ray imaging of mouse using a colloid solution of silica-coated Au (Au/SiO$_2$) nanoparticles. A colloid solution of Au nanoparticles with a size of 16.9 nm was prepared using hydrogen tetrachloroaurate (III) trihydrate as Au source and sodium citrate as reducing reagent. Silica coating of the Au nanoparticles was performed by modifying the Au nanoparticle surface with (3-aminopropyl)trimethoxysilane and then by depositing silica nuclei generated through a sol–gel reaction of tetraethyl orthosilicate in water/ethanol initiated with sodium hydroxide on the surface-modified surface, which produced Au/SiO$_2$ particles with a size of 136.4 nm. A computed tomography value of the Au/SiO$_2$ colloid solution with an Au concentration of 0.036 M was as high as 1,184.8 Hounsfield units, which was quite higher than that of a commercial X-ray contrast agent with the same iodine concentration as the Au concentration. Tissues of mouse could be imaged by injecting the Au/SiO$_2$ particle colloid solution into them.

Keywords: Au; Silica; Core-shell; Nanoparticle; X-ray contrast agent

Background

An X-ray imaging technique is one of the quite useful medical diagnoses [1-3] because internal organs can be imaged without a surgical operation. Images taken with the technique are made clearer using contrast agents that strongly absorb X-ray [4-6]. The contrast agents, which are commercially available, are solutions that dissolve iodine compounds homogeneously in solvents at molecular level. The iodine compound molecules are not strongly dragged in fluid because of their small sizes. Consequently, they cannot stay in internal organs for a long period, which provides difficulty taking steady images. In addition, the iodine-related contrast agents cannot be used for patients in whom iodine compounds provoke adverse events like allergic reactions [7-9].

Gold is a material that has been extensively characterized [10,11]. Gold also absorbs X-ray strongly, which means that it is available for obtaining X-ray images with high contrast. From this viewpoint, studies on the X-ray imaging ability of metallic Au nanoparticles have been performed for development of new contrast agents that aid the technique to image tissues in internal organs at nanometer level [12-20]. The particles have another advantage over gold dissolved homogeneously in solvents at molecular level. The particles are strongly dragged in fluid because of their size which is larger than that of molecules. Thus, their residence time in internal organs will increase, which may allow steady imaging.

Metallic nanoparticles also have troubled us with their toxicity in internal organs [21-28]. Formation of core-shell particles containing Au nanoparticles as the core is a candidate for solving the problem since the shell can keep the particles from contacting with internal organs, which decreases the toxicity of Au nanoparticles. Materials inert for internal organs are desirable as materials for the shell. Silica is one of the promising materials for the shell because it is inert for internal organs compared to iodine compounds and metallic nanoparticles. Several research groups have proposed methods for producing core-shell particles composed of Au nanoparticle core such as spheres, rods, cages, etc. and silica shell, most of which are related to a sol–gel process [29-38]. Our research group has also studied on development of a

* Correspondence: ykoba@mx.ibaraki.ac.jp
[1]Department of Biomolecular Functional Engineering, College of Engineering, Ibaraki University, 4-12-1 Naka-narusawa-cho, Hitachi, Ibaraki 316-8511, Japan
Full list of author information is available at the end of the article

method for silica coating of Au nanoparticles [39-42]. In the developed method, the silica-coated particles were fabricated in three steps. The first, second, and third steps are (1) preparation of the Au nanoparticle colloid solution by reducing hydrogen tetrachloroaurate(III) with sodium citrate in water, (2) modification of the Au nanoparticle surface with hydrophilic groups using a silane coupling agent with an amino group as surface primer, and (3) formation of silica shells on the hydrophilic surface through the sol–gel reaction of silicon alkoxide using sodium hydroxide (NaOH) aqueous solution as a basic catalyst in ethanol, respectively.

The colloid solution of silica-coated Au (Au/SiO_2) nanoparticles with the size of 47.3 nm prepared by the developed method was examined for X-ray imaging of mouse in our previous work [42]. Properties of particles such as colloidal stability and residence time in internal organs should be dependent on the particle size. Au/SiO_2 nanoparticles with not only the size of 47.3 nm but also various sizes were successfully fabricated in another work of ours [40]. The present work examines the colloid solution of Au/SiO_2 nanoparticles with a different size for X-ray imaging of tissues in a mouse to accumulate data useful for optimizing the size of contrast agent particles.

Results and discussion
Morphology of Au/SiO_2 particles
Figure 1a shows a photograph of the concentrated Au/SiO_2 particle colloid solution. A dark red solution was obtained. No flocculation, aggregation, and precipitation were found by passing the solution through a light and then observing it with the naked eyes. This observation showed the high colloidal stability of the concentrated Au/SiO_2 particle colloid solution. A transmission electron microscopy (TEM) image of the Au/SiO_2 particles in the concentrated colloid solution is shown in Figure 1b. The average size of the particles was 136.4 ± 17.8 nm, which was close to that of the as-prepared Au/
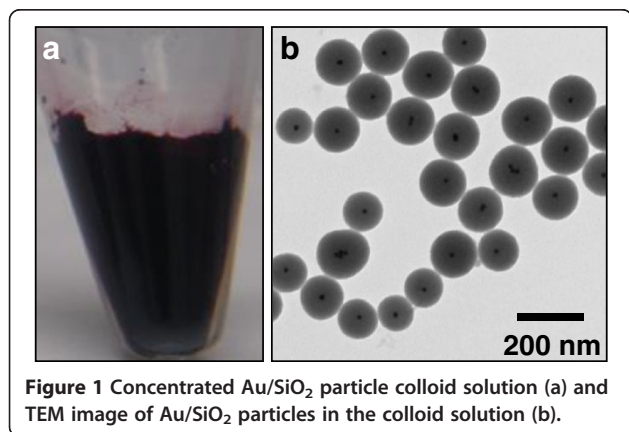

Figure 1 Concentrated Au/SiO_2 particle colloid solution (a) and TEM image of Au/SiO_2 particles in the colloid solution (b).

SiO_2 particles in the prior work. The Au/SiO_2 particles still had a spherical core-shell structure even after the concentrating process, which indicated that the Au/SiO_2 particles produced in the present work were mechanically stable. The inductively coupled plasma (ICP) measurement revealed that an actual Au concentration in the concentrated Au/SiO_2 particle colloid solution was 0.036 M, which indicated that 41.9% of Au contained in the Au nanoparticle colloid solution was consumed for the preparation of the concentrated Au/SiO_2 particle colloid solution.

CT values of the Au/SiO_2 particle colloid solution
Figure 2b,c,d shows X-ray images of Au/SiO_2 particle colloid solutions with different actual Au concentrations. For comparison, an X-ray image of water is also shown. The white contrast of the image increased as the Au concentration increased.

Figure 3 shows the computed tomography (CT) value of the Au/SiO_2 particle colloid solution versus the actual Au concentration. The CT value increased quasi-linearly with an increase in Au concentration and was as high as 1,184.8 Hounsfield units (HU) at an actual Au concentration of 0.036 M. The straight line, which was drawn mathematically by the least squares method of linear regression, had a slope of 3.32×10^4 HU/M. According to our previous work [42], the slope for Iopamiron®300, which is a commercial iodine-related X-ray contrast agent purchased from Bracco Eisai (Bunkyo-ku Tokyo, Japan), was 4.76×10^3 HU/M. The slope for the Au/SiO_2 particle colloid solution was around seven times larger than that for Iopamiron®300. This tendency shown in the present work was similar to studies reported by several researchers that resulted in CT values of Au nanoparticles or clusters higher than commercial iodine compound contrast agents with the same iodine concentration as that of the Au [12,19,43]. The size of gold atom is larger than that of iodine due to its larger atom number, and the absorption coefficient for the X-ray of gold is comparable to that of iodine. This indicates that the projected area of Au nanoparticles in the colloid solution should be larger than that of the iodine compound. Consequently, such a tendency was shown for the Au/SiO_2 particle colloid solution. Accordingly, the present result on its X-ray absorption ability expected the Au/SiO_2 particle colloid solution produced in the present work to function as an X-ray contrast agent.

X-ray imaging of the mouse
Figure 4 shows X-ray images of the mouse prior to and after the injection of the concentrated Au/SiO_2 particle colloid solution. Figure 5 shows CT values of various tissues as a function of time after the injection. CT values at 0 min corresponded to those prior to the injection.
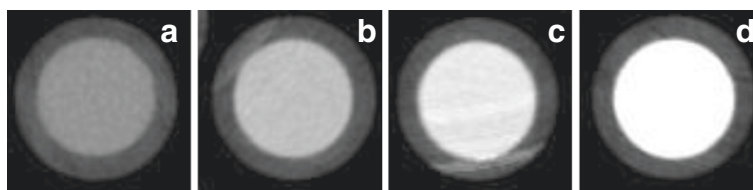
Figure 2 X-ray images of (a) water and (b, c, d) Au/SiO$_2$ particle colloid solutions. The Au concentrations in the colloid solutions were (b) 0.011, (c) 0.020, and (d) 0.036 M.

Prior to the injection, it was hard to recognize tissues such as the liver and the spleen in the images. CT values of the liver and the spleen were 76.7 and 96.5 HU, respectively, at 0 min. The contrasts of these tissues decreased after the injection, compared to those prior to the injection. At 5 min after the injection, their CT values increased markedly up to 115.0 and 120.2 HU, respectively. Then, the values almost leveled out in 240 min (6 h), and they did not remarkably decrease even in 2,880 min (2 days). These tendencies were similar to the results for the Au/SiO$_2$ particles with the size of 47.3 nm that was reported in our previous work [40]; there was no large difference in the dependence of the CT value on time between the Au/SiO$_2$ particle sizes examined. The present results indicated that the Au/SiO$_2$ particles efficiently reached the tissues through a flow in the blood vessels and were trapped in the tissues, and then the tissues could be imaged. For the kidneys, their contrasts were almost constant for all the times examined, in which their CT value was around 65 HU. This indicated that the Au/SiO$_2$ particles were probably recognized as alien substances and were intensively trapped in the liver and the spleen. The internal organs recognize

hydrophobic materials as foreign through interaction between proteins and the hydrophilic surface of the materials [44-48]. The surface of the Au/SiO$_2$ particles seemed to be hydrophilic because of silanol groups derived from the silica surface of Au/SiO$_2$ particles. The trapping took place for the liver and the spleen with the hydrophilic surface. Accordingly, these results proved that the Au/SiO$_2$ particle surface was required to be more hydrophilic for improving their imaging function.

Conclusions

The Au/SiO$_2$ particles with the average size of 138.9 ± 12.4 nm and the Au core size of 16.9 ± 1.2 nm that were fabricated in our previous work were applied to X-ray imaging in the present work. The actual Au concentration of the Au/SiO$_2$ particle colloid solution was 0.036 M after concentrated to 1/2,000 of its original volume. The concentrated Au/SiO$_2$ particle colloid solution had the CT value of 1,184.8 HU. This value was high compared to that for the commercial X-ray contrast agent with the same iodine concentration as the Au concentration, which indicated that the Au/SiO$_2$ particle colloid solutions were sensitive for absorption of X-ray. The injection of the colloid solution into a mouse made the X-ray images of its internal organs such as the liver and spleen taken clearly. Accordingly, the Au/SiO$_2$ particle colloid solution was proved to be able to work as an X-ray contrast agent. Further studies, in particular on the toxicity of particle colloid solutions, are in progress toward practical use.

Methods

Chemicals

Au nanoparticles were prepared from hydrogen tetrachloroaurate(III) trihydrate (HAuCl$_4$·3H$_2$O, >98%, Kanto Chemical, Chuo-ku, Tokyo, Japan) as an Au source and trisodium citrate dihydrate (Na-cit, 99%, Kanto Chemical) as a reducing reagent. (3-Aminopropyl) trimethoxysilane (APMS, 97%, Sigma-Aldrich, St. Louis, MO, USA) were used as a silane coupling agent for increasing the affinity between the Au particle surface and silica shell. Tetraethyl orthosilicate (TEOS, 95%, Kanto Chemical), sodium hydroxide (NaOH) aqueous solution (1 mol/L, Kanto Chemical), and ethanol (99.5%, Kanto
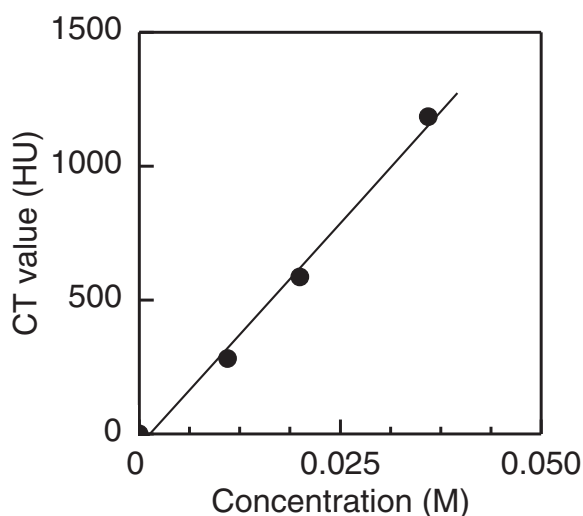

Figure 3 CT value versus Au concentration of the AuSiO$_2$ particle colloid solution.
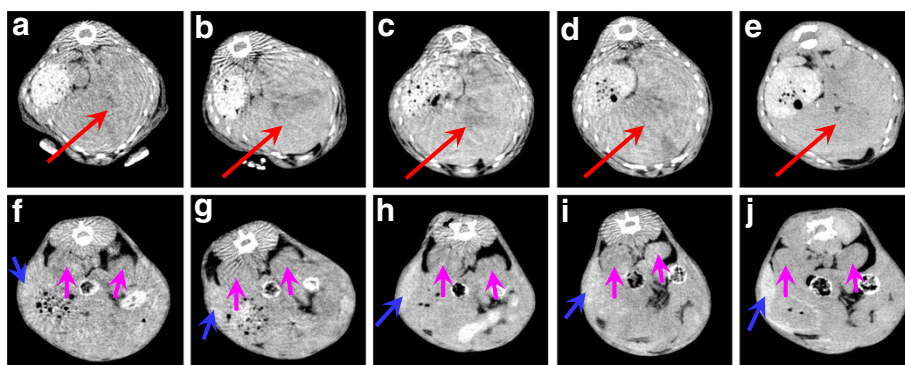
Figure 4 CT images of the internal organs of the mouse after injection. CT images of the liver (red arrows), spleen (blue arrows), and kidney (pink arrows) of the mouse after injection of Au/SiO₂ particle colloid solution. The Au concentration in the colloid solution and the volume of the injected colloid solution were 0.036 M and 80 μL, respectively. The images were taken **(a, f)** prior to injection and at **(b, g)** 5, **(c, h)** 360, **(d, i)** 1,440, and **(e, j)** 2,880 min after injection.

Chemical) were used as a silica source, a catalyst for the sol–gel reaction of TEOS, and a solvent for silica coating, respectively. Hydrofluoric acid (HF, 46.0% to 48.0%, Kanto Chemical), nitric acid (HNO_3, 69% to 70%, Kanto Chemical), and hydrochloric acid (HCl, 35.0% to 37.0%, Kanto Chemical) were used for preparing samples for ICP spectrometry. All chemicals were used as received. Water that was ion-exchanged and distilled with Yamato WG-250 (Koto-ku, Tokyo, Japan) was used in all the preparation.

Preparation of materials

A colloid solution of Au/SiO₂ particles was prepared in two steps, as reported in our previous work [40]. The first step was preparation of the Au nanoparticle colloid solution. The preparation was performed by adding a

Figure 5 CT values of the internal organs of the mouse after injection. CT values of the liver (filled circle), spleen (empty circle), and kidney (triangle) of the mouse as a function of time after injection of Au/SiO₂ particle colloid solution. The Au concentration in the colloid solution and the volume of the injected colloid solution were 0.036 M and 80 μL, respectively.

Na-cit aqueous solution to an $HAuCl_4$ aqueous solution at a constant temperature of 80°C under vigorous stirring. Initial concentrations of Au and Na-cit were 2.4×10^{-4} and 1.6×10^{-3} M, respectively. The total volume of the final reactant solution was 400 mL. Production of Au nanoparticles was implied with visual observation for color change of the solution to wine red after the addition. According to TEM, the Au nanoparticles had a volume-average size of 16.9 ± 1.2 nm [40]. The second step was silica coating of the obtained Au nanoparticles. The silica coating was performed by a sol–gel method in the presence of Au nanoparticles. At 15 min after addition of an APMS aqueous solution to the obtained Au nanoparticle colloid solution, ethanol and TEOS were successively added to the colloid solution. The following rapid injection of an NaOH aqueous solution into the Au/TEOS colloid solution initiated a sol–gel reaction of TEOS or the silica coating. The reaction temperature and time were 35°C and 24 h, respectively. The total volume of the final reactant solution was 2,000 mL. Initial concentrations of Au, APMS, NaOH, H₂O, and TEOS in the final reactant solution were adjusted to 4.3×10^{-5}, 2.0×10^{-5}, 1.0×10^{-3}, 10.7, and 1.0×10^{-2} M, respectively. TEM observation indicated that these initial concentrations resulted in production of Au/SiO₂ particles with a volume-average particle size of 138.9 ± 12.4 nm [40].

Characterization

TEM was used for investigation of the morphology of the particles. TEM observation was performed with a JEOL JEM-2000FX II microscope (Akishima-shi, Japan) operating at 200 kV. To prepare samples for TEM, the particle colloid solution was dropped on a collodion-coated copper grid, and then its dispersion medium was evaporated in air followed by *in vacuo*. Volume-average particle sizes were determined by measuring dozens of particle
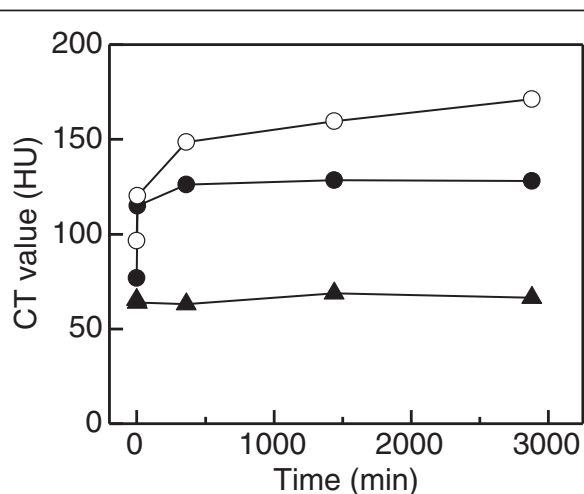
diameters in TEM images. An actual Au concentration of the concentrated Au/SiO_2 particle colloid solution was determined by ICP. A Shimadzu ICPS-7510 emission spectrometer (Kyoto, Japan) was used for the ICP. To prepare samples for the ICP, HF and aqua regia composed of 1:3 (v/v) HNO_3/HCl were successively added to the concentrated Au/SiO_2 particle colloid solution to dissolve the silica shell and Au nanoparticles, respectively. Then, the obtained solution was diluted to adjust the Au concentration to a concentration appropriate to the ICP measurement. X-ray images and CT values of samples such as Iopamiron®300, the Au/SiO_2 particle colloid solution, and a mouse injected with the particle colloid solutions were obtained with the Aloka LaTheta LCT-200 CT system (Mitaka-shi, Japan), according to our previous work [42]. Prior to the measurement of the CT value for the Au/SiO_2 particle colloid solution, the Au/SiO_2 particles were washed by salting out the Au/SiO_2 particles with addition of a saturated NaCl aqueous solution, removing the supernatant by decantation, and then repeating a washing process composed of centrifugation, removal of the supernatant, addition of water, and shaking with a vortex mixer for several times. The Au/SiO_2 particle colloid solution was concentrated to 1/2,000 of its original volume by decreasing the amount of added water in the washing process (concentrated Au/SiO_2 particle colloid solution). Assuming complete reduction of $HAuCl_4$ to metallic Au and no loss of particles during the concentrating process, the concentrated Au/SiO_2 particle colloid solution was considered to have an initial Au concentration of 0.086 M. The samples were put into a tube with a diameter of 3.7 cm and a length of 29.5 cm. The images were taken as if the samples were cut into round slices. CT values of samples were estimated with the basis of CT values of −1,000 HU for air and 0 HU for water. The mouse used was the ICR mouse with the age of 5 to 6 weeks old. The mouse was put under anesthesia, and 80 μL of the colloid solution was injected into the mouse from its tail veins. All sugical processes were performed for the mouse under anesthesia in accordance with guidelines approved by the committee on animal experiments of Tohoku University.

Competing interests

The authors declare that they have no competing interests.

Authors' contributions

YK (Kobayashi) drafted the manuscript. KG and NO modified it. HI, TN, and YK (Kubota) participated in some practical work. All authors read and approved the final manuscript.

Acknowledgements

Author details

[1]Department of Biomolecular Functional Engineering, College of Engineering, Ibaraki University, 4-12-1 Naka-narusawa-cho, Hitachi, Ibaraki 316-8511, Japan. [2]Division of Surgical Oncology, Graduate School of Medicine, Tohoku University, Seiryo-machi, Aoba-ku, Sendai, Miyagi 980-8574, Japan.

References

1. Bellani, G, Caironi, P: Lung imaging during acute respiratory distress syndrome: CT- and PET-scanning. Trends Anaesth Crit Care **1**, 203–209 (2011)
2. Duwek, HC, Spitzer, H, Weitzen, R, Apter, S: A biologically-based algorithm for companding computerized tomography (CT) images. Comput Biol Med **41**, 367–379 (2011)
3. Ruschin, M, Komljenovic, PT, Ansell, S, Ménard, C, Bootsma, G, Cho, YB, Chung, C., Jaffray, D: Cone beam computed tomography image guidance system for a dedicated intracranial radiosurgery treatment unit. Int J Radiat Oncol Biol Phys **85**, 243–250 (2013)
4. Lee, SJ, Jung, SY, Ahn, S: Flow tracing microparticle sensors designed for enhanced X-ray contrast. Biosens Bioelectron **25**, 1571–1578 (2010)
5. Hwang, UJ, Shin, DH, Kim, TH, Moon, SH, Lim, YK, Jeong, H, Rah, JE, Kim, SS, Kim, JY, Kim, DY, Park, SY, Cho, KH: The effect of a contrast agent on proton beam range in radiotherapy planning using computed tomography for patients with locoregionally advanced lung cancer. Int J Radiat Oncol Biol Phys **81**, e317–e324 (2011)
6. Rustighi, I, Donati, I, Ferluga, M, Campa, C, Pasqua, AE, Rossib, M, Paoletti, S: Borate complexes of X-ray iodinated contrast agents: characterization and sorption studies for their removal from aqueous media. J Hazard Mater **205–206**, 10–16 (2012)
7. Thomsen, HS: Contrast media safety - an update. Eur J Radiol **80**, 77–82 (2011)
8. Ichikawa, T, Motosugi, U, Morisaka, H, Sou, H, Onohara, K, Sano, K, Araki, T: Optimal iodine dose for 3-dimensional multidetector-row CT angiography of the liver. Eur J Radiol **81**, 2450–2455 (2012)
9. Li, X, Anton, N, Zuber, G, Zhao, M, Messaddeq, N, Hallouard, F, Fessi, H, Vandamme, TF: Iodinated a-tocopherol nano-emulsions as non-toxic contrast agents for preclinical X-ray imaging. Biomater **34**, 481–491 (2013)
10. Malarkodi, C, Rajeshkumar, S, Vanaja, M, Paulkumar, K, Gnanajobitha, G, Annadurai, G: Eco-friendly synthesis and characterization of gold nanoparticles using *Klebsiella pneumoniae*. J Nanostruct Chem **3**, 30 (2013)
11. Rajeshkumar, S, Malarkodi, C, Gnanajobitha, G, Paulkumar, K, Vanaja, M, Kannan, C, Annadurai, G: Seaweed-mediated synthesis of gold nanoparticles using *Turbinaria conoides* and its characterization. J Nanostruc Chem **3**, 44 (2013)
12. Park, JA, Kim, HK, Kim, JH, Jeong, SW, Jung, JC, Lee, GH, Lee, J, Chang, Y, Kim, TJ: Gold nanoparticles functionalized by gadolinium-DTPA conjugate of cysteine as a multimodal bioimaging agent. Bioorg Med Chem Lett **20**, 2287–2291 (2010)
13. Cho, EC, Glaus, C, Chen, J, Welch, MJ, Xia, Y: Inorganic nanoparticle-based contrast agents for molecular imaging. Trends Mol Med **16**, 561–573 (2010)
14. Wang, H, Zheng, L, Peng, C, Guo, R, Shen, M, Shi, X, Zhang, G: Computed tomography imaging of cancer cells using acetylated dendrimer-entrapped gold nanoparticles. Biomater **32**, 2979–2988 (2011)
15. Ahn, S, Jung, SY, Seo, E, Lee, SJ: Gold nanoparticle-incorporated human red blood cells (RBCs) for X-ray dynamic imaging. Biomater **32**, 7191–7199 (2011)
16. Menk, RH, Schültke, E, Hall, C, Arfelli, F, Astolfo, A, Rigon, L, Round, A, Ataelmannan, K, MacDonald, SR, Juurlink, BHJ: Gold nanoparticle labeling of cells is a sensitive method to investigate cell distribution and migration in animal models of human disease. Nanomed Nanotechnol Biol Med **7**, 647–654 (2011)
17. Roessl, E, Cormode, D, Brendel, B, Engel, KJ, Martens, G, Thran, A, Fayad, Z, Proks, R: Preclinical spectral computed tomography of gold nano-particles. Nucl Instrum Met Phys Res A **648**, S259–S264 (2011)
18. Zhang, XD, Wu, D, Shen, X, Chen, J, Sun, YM, Liu, PX, Liang, XJ: Size-dependent radiosensitization of PEG-coated gold nanoparticles for cancer radiation therapy. Biomater **33**, 6408–6419 (2012)
19. Peng, C, Zheng, L, Chen, Q, Shen, M, Guo, R, Wang, H, Cao, X, Zhang, G, Shi, X: PEGylated dendrimer-entrapped gold nanoparticles for in vivo blood pool and tumor imaging by computed tomography. Biomater **33**, 1107–1119 (2012)
20. Kim, D, Jon, S: Gold nanoparticles in image-guided cancer therapy. Inorg Chim Acta **393**, 154–164 (2012)

21. Tedesco, S, Doyle, H, Blasco, J, Redmond, G, Sheehan, D: Oxidative stress and toxicity of gold nanoparticles in *Mytilus edulis*. Aquat Toxicol **100**, 178–186 (2010)
22. Ahamed, M, AlSalhi, MS, Siddiqui, MKJ: Silver nanoparticle applications and human health. Clin Chim Acta **411**, 1841–1848 (2010)
23. Farkas, J, Christian, P, Urrea, JAG, Roos, N, Hasellöv, M, Tollefsen, KE, Thomas, KV: Effects of silver and gold nanoparticles on rainbow trout (*Oncorhynchus mykiss*) hepatocytes. Aquat Toxicol **96**, 44–52 (2010)
24. Lasagna-Reeves, C, Gonzalez-Romero, D, Barria, MA, Olmedo, I, Clos, A, Ramanujam, VMS, Urayama, A, Vergara, L, Kogan, MJ, Soto, C: Bioaccumulation and toxicity of gold nanoparticles after repeated administration in mice. Biochem Biophys Res Commun **393**, 649–655 (2010)
25. Han, X, Gelein, R, Corson, N, Mercer, PW, Jiang, J, Biswas, P, Finkelstein, JN, Elder, A, Oberdörster, G: Validation of an LDH assay for assessing nanoparticle toxicity. Toxicol **287**, 99–104 (2011)
26. Park, MVDZ, Neigh, AM, Vermeulen, JP, de la Fonteyne, LJJ, Verharen, HW, Briedé, JJ, Van Loveren, H, De Jong, WH: The effect of particle size on the cytotoxicity, inflammation, developmental toxicity and genotoxicity of silver nanoparticles. Biomater **32**, 9810–9817 (2011)
27. Schulz, M, Ma-Hock, L, Brill, S, Strauss, V, Treumann Gröters, SS, van Ravenzwaay, B, Landsiedel, R: Investigation on the genotoxicity of different sizes of gold nanoparticles administered to the lungs of rats. Mutat Res **745**, 51–57 (2012)
28. Nymark, P, Catalán, J, Suhonen, S, Järventaus, H, Birkedal, R, Clausen, PA, Jensen, KA, Vippola, M, Savolainena, K, Norppa, H: Genotoxicity of polyvinylpyrrolidone-coated silver nanoparticles in BEAS 2B cells. Toxicol in press
29. Lu, Y, Yin, Y, Li, ZY, Xia, Y: Synthesis and self-assembly of Au@SiO$_2$ core-shell colloids. Nano Lett **2**, 785–788 (2002)
30. Xu, J, Perry, CC: A novel approach to Au@SiO$_2$ core-shell spheres. J Non-Cryst Solid **353**, 1212–1215 (2007)
31. Ye, J, Broek, BV, Palma, RD, Libaers, W, Clays, K, Roy, WV, Borghs, G., Maes, G: Surface morphology changes on silica-coated gold colloids. Colloids Surf A **322**, 225–233 (2008)
32. Wu, Z, Liang, J, Ji, X, Yang, W: Preparation of uniform Au@SiO$_2$ particles by direct silica coating on citrate-capped Au nanoparticles. Colloids Surf A **392**, 220–224 (2011)
33. Wang, TT, Chai, F, Wang, CG, Li, L, Liu, HY, Zhang, LY: Fluorescent hollow/rattle-type mesoporous Au@SiO$_2$ nanocapsules for drug delivery and fluorescence imaging of cancer cells. J Colloid Inter Sci **358**, 109–115 (2011)
34. Huang, CC, Huang, CH, Kuo, IT, Chau, LK, Yang, TS: Synthesis of silica-coated gold nanorod as Raman tags by modulating cetyltrimethylammonium bromide concentration. Colloids Surf A **409**, 61–68 (2012)
35. Yu, D, Zeng, Y, Qi, Y, Zhou, T, Shi, G: A novel electrochemical sensor for determination of dopamine based on AuNPs@SiO$_2$ core-shell imprinted composite. Biosens Bioelectron **38**, 270–277 (2012)
36. Fülöp, E, Nagy, N, Deák, A, Bársony, I: Langmuir–Blodgett films of gold/silica core/shell nanorods. Thin Solid Films **520**, 7002–7005 (2012)
37. Shen, S, Tang, H, Zhang, X, Ren, J, Pang, Z, Wang, D, Gao, H, Qian, Y, Jiang, X, Yang, W: Targeting mesoporous silica-encapsulated gold nanorods for chemo-photothermal therapy with near-infrared radiation. Biomater **34**, 3150–3158 (2013)
38. Khlebtsov, BN, Khanadeev, VA, Panfilova, EV, Inozemtseva, OA, Burov, AM, Khlebtsov, NG: A simple Mie-type model for silica-coated gold nanocages. J Quant Spectrosc Ra **121**, 23–29 (2013)
39. Mine, E, Yamada, A, Kobayashi, Y, Konno, M, Liz-Marzán, LM: Direct coating of gold nanoparticles with silica by a seeded polymerization technique. J Colloid Interface Sci **264**, 385–390 (2003)
40. Kobayashi, Y, Inose, H, Nakagawa, T, Gonda, K, Takeda, M, Ohuchi, N, Kasuya, A: Control of shell thickness in silica-coating of Au nanoparticles and their X-ray imaging properties. J Colloid Interface Sci **358**, 329–333 (2011)
41. Kobayashi, Y, Inose, H, Nakagawa, T, Gonda, K, Takeda, M, Ohuchi, N, Kasuya, A: Synthesis of Au-silica core-shell particles by sol–gel process. Surf Eng **28**, 129–133 (2012)
42. Kobayashi, Y, Inose, H, Nagasu, R, Nakagawa, T, Kubota, Y, Gonda, K, Ohuchi, N: X-ray imaging technique using colloid solution of Au/silica/poly(ethylene glycol) nanoparticles. Mater Res Innov in press
43. Zhang, A, Tu, Y, Qin, S, Li, Y, Zhou, J, Chen, N, Lu, Q, Zhang, B: Gold nanoclusters as contrast agents for fluorescent and X-ray dual-modality imaging. J Colloid Interface Sci **372**, 239–244 (2012)
44. Hallouard, F, Anton, N, Choquet, P, Constantinesco, A, Vandamme, T: Iodinated blood pool contrast media for preclinical X-ray imaging applications - a review. Biomater **31**, 6249–6268 (2010)
45. Parveen, S, Sahoo, SK: Long circulating chitosan/PEG blended PLGA nanoparticle for tumor drug delivery. Eur J Pharmacol **670**, 372–383 (2011)
46. Dufort, S, Sancey, L, Coll, JL: Physico-chemical parameters that govern nanoparticles fate also dictate rules for their molecular evolution. Adv Drug Deliv Rev **64**, 179–189 (2012)
47. Stolnik, S, Illum, L, Davis, SS: Long circulating microparticulate drug carriers. Adv Drug Deliv Rev **64**, 290–301 (2012)
48. Bauer, S, Schmuki, P, von der Mark, K, Park, J: Engineering biocompatible implant surfaces: part I: materials and surfaces. Prog Mater Sci **58**, 261–326 (2013)